The Effect of Pores on Compressive Failure of Highly Aligned Carbon Fibre Reinforced Epoxy Composite Rods Produced by Pultrusion

C.J.Creighton and T.W.Clyne

Department of Materials Science and Metallurgy
University of Cambridge
Pembroke Street, Cambridge, CB2 3QZ, U.K.

SUMMARY: Compressive strengths have been measured for two grades of pultruded epoxy - 67vol% carbon fibre composite. Differences in the pultrusion conditions for the two grades led to relatively high porosity levels in the interior of one of them, while the other was effectively pore-free. Both exhibited excellent fibre alignment. Despite this, initial measured strengths were relatively low (~1.7-1.8 GPa), with little difference between the values obtained for the two grades. This is explained, with the help of FEM modeling work, as being due to the generation of stress concentrations near the end of the gauge length at the specimen periphery, where the two grades exhibited similar (pore-free) microstructures. Further measurements indicated that the true strengths were about 2.7-2.8 GPa for the pore-free material and about 2.1 GPa for the porous material. These values are broadly consistent with the expected effect of the presence of the pores, which tend to promote shearing parallel to the fibre axis, leading to formation of kink bands and consequent failure.

1. INTRODUCTION

Composite strengths under compressive loading parallel to the fibre axis are usually lower than when the same material is loaded in tension. Most models for compressive strength relate to shear failure parallel to the fibre axis, which occurs more readily with increasing misalignment between this direction and the loading axis. The presence of a region in which the fibres are misoriented with respect to the loading axis by an angle ϕ leads to failure via formation of a *kink band* (sometimes termed a *microbuckle*) at an applied stress σ_k*, which can be related to a critical interfacial shear stress on planes parallel to the fibre axis, $\tau_{12}*$. The value of $\tau_{12}*$ should be measured experimentally on the composite material concerned, although it may be close to the matrix shear yield stress in some cases. Writing ϕ as the sum of an original misorientation ϕ_0 and the elastic shear strain, γ_{12}, arising from the shear stress $\tau_{12}*$ leads, after some rearrangement, to the following expression for the compressive strength.

$$\sigma_{k*} = \left(\frac{1}{G_{12c}} + \frac{\phi_0}{\tau_{12*}} \right)^{-1} \qquad (1)$$

where G_{12c} is the shear modulus of the composite.

An analysis of this type has been presented by Budiansky and Fleck[1]. The above equation reduces to expressions derived earlier by Argon[2] and by Rosen[3] for the respective limiting cases of a rigid-plastic material ($G_{12c} \to \infty$) and no initial fibre misalignment ($\phi_0 \to 0$). The equation predicts a value for σ_k* which falls sharply with increasing ϕ_0 from G_{12c} (typically

several GPa for a polymer matrix composite) at $\phi_0 = 0^\circ$ to about 1-2 GPa at $\phi_0 \approx 2\text{-}3^\circ$, for a composite shear strength, $\tau_{12}*$, of around 50-100 MPa.

A few researchers[5,14-18] have considered the possibility of the behaviour being affected by the strength of the fibres. In a recent study[18] of monofilament-reinforced titanium, for which low values of ϕ_0 are readily attainable and the shear strength τ_{12*} is relatively high (~300 MPa), it was shown that there is a range of ϕ_0 (up to about 3˚) for which failure occurs by a fibre crushing mechanism, such that the composite compressive strength is approximately constant and is given by the following equation

$$\sigma_{c*} = \frac{f\sigma_{f*} + (1-f)\sigma_{mY}}{\cos^2 \phi_0} \qquad (2)$$

where f is the fibre volume fraction, σ_f* is the fibre crushing strength and σ_{mY} is the matrix yield strength. A consequence of the relatively low shear strengths and shear moduli of polymer composites is that the compressive strength indicated by eqn.(1) is normally well below that given by eqn.(2) for these materials, although, in view of uncertainties about the compressive strength of many fibres, it is conceivable that this might not be true in cases of very good fibre alignment ($\phi_0 < 1^\circ$) and/or relatively low fibre volume fractions.

2. EXPERIMENTAL PROCEDURES

2.1 Material Production

'Graphlite®' rod, supplied by Neptco Incorporated, was produced using a pultrusion technique. The composite comprises about 67vol.% of IM7 carbon fibres, in an "Epon" range epoxy resin matrix. The product was in the form of continuous rod with a diameter of 1.7 mm. Two grades of material were supplied, termed grade A and grade B. These were produced using different pultrusion conditions. Although the processing details are not available, grade B was produced under conditions allowing a more rapid production rate than grade A: a consequence of this was that grade B contained higher levels of internal defects, most noticeably in the form of relatively high porosity levels - primarily associated with the ends of fractured fibres.

2.2 Microstructural Examination

As-received rods were sectioned normal and parallel to the fibre direction, using an Isomet low speed saw. Samples were mounted and polished, using standard metallographic techniques, and subsequently examined using optical and scanning electron microscopy. Typical micrographs of transverse sections are shown in Fig.1 for the two grades of composite. While there is no obvious porosity in the grade A material, grade B has a relatively high incidence of pores. These pores are concentrated towards the central regions. Study of axial sections revealed that they are considerably elongated in the pultrusion direction, with a typical aspect ratio of about 20.

Densitometry was used to quantify the pore volume fraction in each grade of material. This involved hydrostatic weighing of specimens in two media (air and Flutec PP9, ie perfluoro-1-methyl decalin), using a Sartorius YDK 01-0D balance (precision ±10 µg). Specimen densities were established from measured apparent weights and the density of the two media. Pore volume fractions were then estimated using handbook densities and measured volume fractions of the two constituents. These results indicate that the average pore content in grade B material was around 3.6%, while that in grade A was about 0.3%.

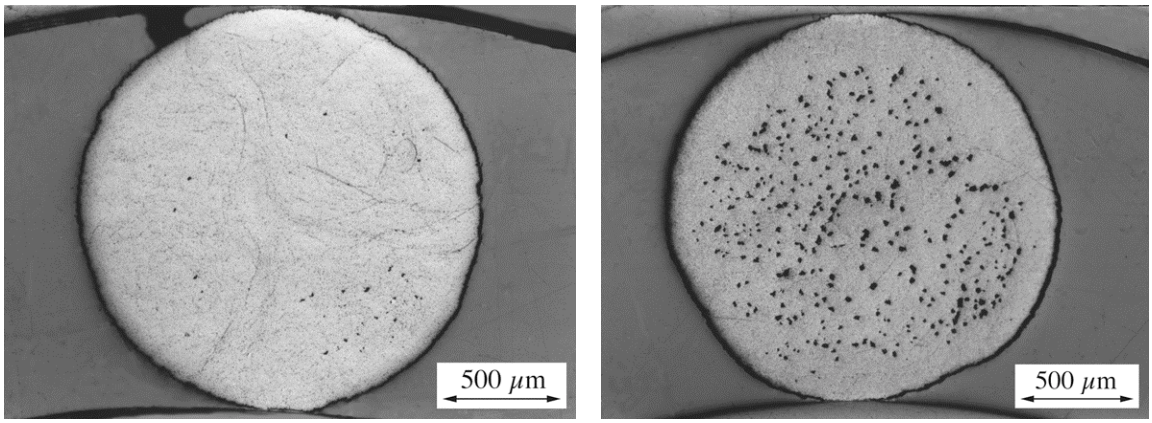

(a) (b)

Figure 1 Optical micrographs of transverse sections from (a) grade A and (b) grade B.

A standard image analysis package was used to measure the fibre volume fraction on several low-magnification SEM images of transverse sections. These measurements indicated an average value of 67% ±1% for all of the specimens examined, which is within the range indicated by the manufacturers.

2.3 Compression Testing

Avoidance of specimen buckling (elastic or plastic) is an important issue. The Shanley treatment[22,23] was used to predict the inelastic buckling stress, σ_b*, as a function of specimen slenderness ratio, *s*, using the correction for shear deformation given by Timoshenko and Gere[24] and the Eshelby method[25,26] to estimate the values of the composite yield stress, σ_{Yc}, and the tangent moduli. Full details are given elsewhere[27]. The gauge length was standardized at 5 mm, corresponding to a slenderness ratio of about 12, which is below the value at which plastic buckling is predicted to occur with the maximum levels of applied stress used in this work.

Samples of the rods supplied were cut to approximately 65 mm lengths, comprising a central gauge length of 5 mm and 30 mm lengths on either side, to be embedded into the loading support system. Strain gauges (1 mm by 1.3 mm) were bonded on the surface of the gauge length, aligned parallel to the loading axis, one located 180˚ around the specimen periphery from the other. In some cases, a gauge oriented transverse to the loading axis was located next to an axial one, allowing the axial-transverse Poisson ratio, ν_{12}, to be measured. The 30 mm embedded lengths were washed in acetone, coated with epoxy adhesive and located into holes drilled along the axes of two 30 mm long cylinders of mild steel. These cylinders were then assembled into the arrangement shown in Fig.2. The assembly was then left for 24 hours while the adhesive cured in situ. This geometry is such that transfer of compressive load to the specimen occurs both through the specimen ends and via shear loading of the lateral faces. All testing was carried out under displacement control, with a strain rate of 3.3×10^{-3} s^{-1}, using a 10 kN ESH mechanical testing machine. Elastic constants obtained experimentally during the tests are compared with predicted values in Table I.

Since FEM analysis (see §4.1) indicated that there were regions of high stress concentration at the specimen periphery near the end of the gauge length, further experiments were carried out in which this stress concentration effect was reduced by cutting down the specimen diameter (from 1.7 mm to 1.2 mm), thus increasing the thickness of the adhesive layer bonding the specimen to the constraining mild steel cylinder.

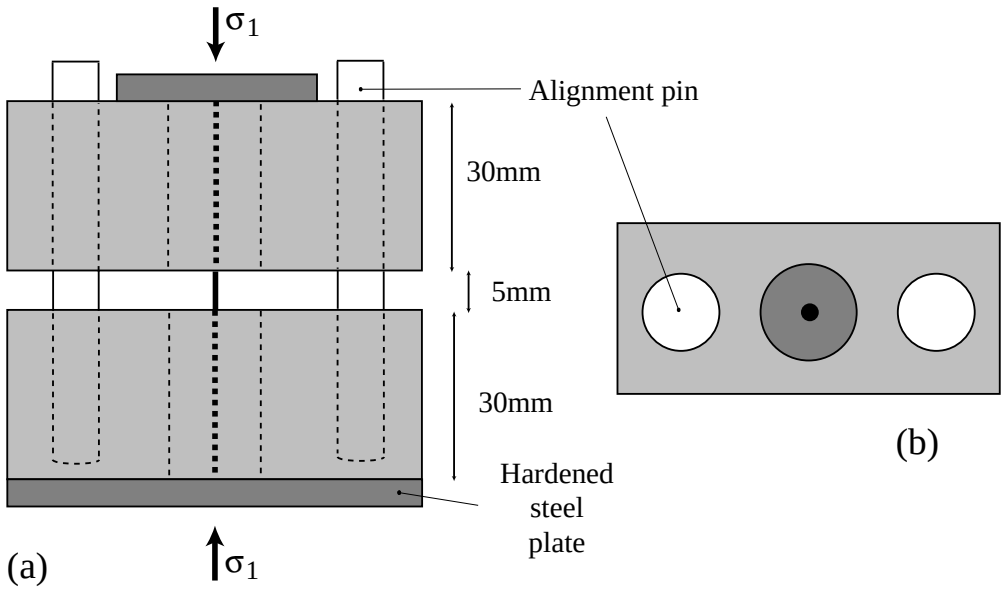

Figure 2 Dimensions of the testing arrangement, showing (a) elevation and (b) plan views.

Specimen diameter reduction, which also had the effect of removing the outer pore-free layer from the grade B specimens, was carried out by cylindrical grinding. For these tests, the gauge length was reduced from 5 mm to 2.5 mm, in order to ensure that there was no danger of buckling.

Table I Elastic constants, taken from the literature[28,29], obtained by calculation (based on a fibre volume fraction of 67% and using Halpin-Tsai expressions, with ξ = 1, and the Eshelby model) and measured experimentally.

	Fibre	Matrix	Composite			Steel
			predicted	grade A	grade B	
Axial modulus, E_1 (GPa)	285	3.04	189.12	178.4	174.3	208
Transverse modulus, E_2 (GPa)	15	3.04	7.9	-	-	208
Poisson ratio, ν_{12}	0.25	0.37	0.28	~0.28	~0.28	0.33

3. COMPRESSIVE FAILURE BEHAVIOUR

A typical stress-strain plot is presented in Fig.3, which also shows the transverse (hoop) strain as a function of axial strain, indicating how the instantaneous Poisson ratio was changing as the test progressed. It can be seen that no significant divergence occurred between the readings of the two axial gauges. This indicates that little or no long range bending of the specimen occurred up to the point of failure. In fact, bending in the plane normal to that defined by the two gauges would not be picked up by these measurements, but the absence of noticeable divergence between pairs of readings for all the tests carried out does indicate that Euler buckling was avoided. It is also clear that the onset of inelastic behaviour precedes failure by a considerable margin. It can be seen in the stress-strain plot that there is a departure from linearity at a strain of about -0.5%. This is confirmed by the data from the transverse gauge, since the Poisson ratio rises at around this point, which is also indicative of some plastic deformation taking place. The value for ν_{12} of about 0.28, recorded in the elastic regime, is consistent with that calculated from the Poisson ratios of the constituents, using the Eshelby method (see Table I).

Figure 4 shows a micrograph of a section through a typical specimen after failure. The fracture surface is fairly smooth and lies at an angle of about 20˚ to the transvese plane. Also visible are well-defined kink bands, which are inclined at similar angles. A tendency was observed for pairs of kink bands to intersect the free surface at the same point, suggesting preferential nucleation at the free surface. This is consistent with recent observations made on metal matrix composites[18]. It is clear that failure occurred as a result of kink band formation, and the fracture plane in this specimen is located where a kink band formed immediately prior to failure. In virtually all cases with the original specimen dimensions and testing geometry, the fracture plane was located at the junction between the gauge length and one of the two gripped sections. For these specimens, mean strengths of 1.78 GPa and 1.67 GPa were obtained for grade A and grade B material respectively, each of these values being from a set of 10 tests.

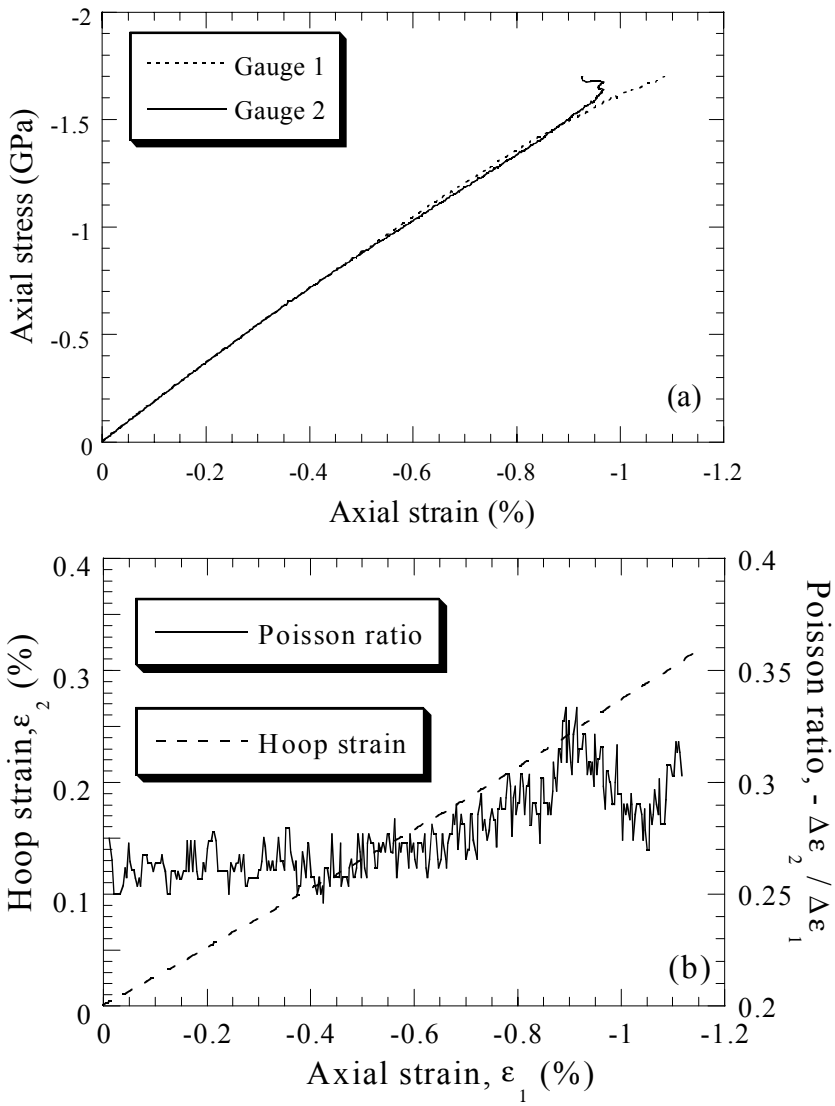

Figure 3 Typical stress - strain data : (a) axial stress-strain plot and (b) dependence of transverse strain on axial strain, together with corresponding variation of the Poisson ratio.

With the specimens of reduced diameter, on the other hand, it was observed that the location of the failure event was more randomly distributed, although still with a tendency to occur near the grips. Microstructural examinations again revealed the presence of kink bands. Mean strength values for these specimens were 2.08 GPa and 1.59 GPa respectively for grade A and grade B material.

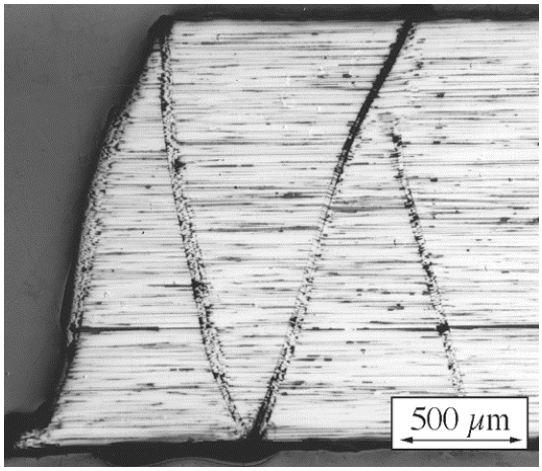

Figure 4 Optical micrograph of a longitudinal section through a failed specimen, showing kink bands

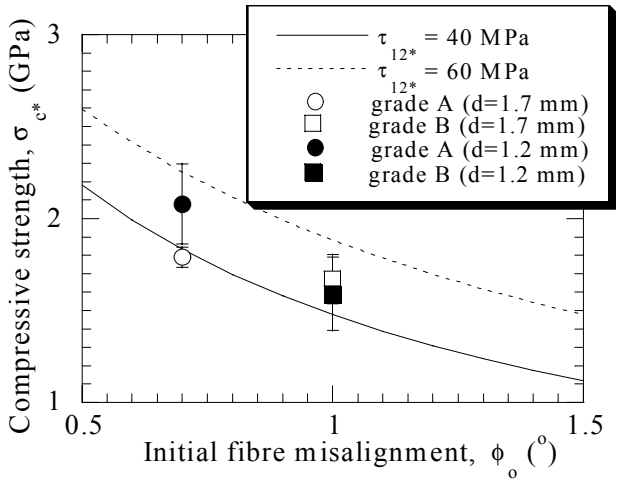

Figure 5 Strength data, plotted at measured (max.) ϕ_0 values, plus predicted plots from eqn.(1), using G_{12} = 1.11 GPa.

Strength data from both types of test are presented in Fig.5, together with predicted plots of the stress for kink band formation as a function of fibre misalignment angle, for two composite shear strength values. It may be noted that a shear strength of the order of 50 MPa would be typical of this type of composite. These results are considered below in the light of an investigation of the stress fields generated during testing.

4. FEM ANALYSIS

Finite element modeling, using ABAQUS v.5.7, was employed to determine elastic stress distributions within the specimen and around individual pores. Meshes were composed of isoparametric 8-noded quadrilateral elements, specially designed for the ABAQUS solver to model axisymmetric systems. The composite material was treated as an anisotropic continuum and the other constituents as isotropic continua. The steel cylinder and steel loading platen remained elastic during loading. The adhesive layer was treated as elasto-plastic, obeying the Ramberg-Osgood relation in shear

$$\gamma = \frac{\tau}{G}\left(1 + \frac{3}{7}\left(\frac{\tau}{\tau_Y}\right)\right)^{n-1} \qquad (3)$$

in which G is given by $E/(2(1+\nu))$, E = 3.5 GPa, ν = 0.4, $\tau_Y = \sigma_Y / \sqrt{3}$ = 35 MPa and n = 3.

4.1 Effect of Test Geometry

The mesh shown in Fig.6 was used to model the effect of the loading arrangement. The interfaces between specimen and adhesive, and between adhesive and cylinder, were assumed to be perfectly bonded. Various gripping arrangement geometries were examined, with particular attention being paid to the effect of the thickness of the adhesive layer. In order to simulate the application of load, a specified force was applied to the loading platen. The base of the specimen, adhesive layer, and cylinder were constrained to experience the same displacement in the loading direction as the loading platen, but relative motion was allowed in the transverse direction. The input data used are given in Table I.

In all cases, a stress concentration effect was observed within the specimen near its periphery, peaking in the region of entry into the steel cylinder - see Fig.6(b). The strength of this effect was reduced as the adhesive layer thickness was increased. This is illustrated in Fig.7, which shows the maximum axial stress in the specimen as a function of the thickness of the adhesive

layer. It can be seen that the original loading geometry, in which the adhesive layer thickness was about 40 μm, would lead to a substantial stress concentration effect ($\sigma \approx 1.6\ \sigma_A$), whereas with the modified geometry (layer thickness ~ 300 μm), this factor would have fallen to about 1.3.

Taking this factor into account, the true strength of the grade A material could be deduced from the original tests ($d = 1.7$ mm) to be of the order of $1.78 \times 1.6 \approx 2.8$ GPa, whereas the tests with the modified design ($d = 1.2$ mm) suggest a value of about $2.08 \times 1.3 \approx 2.7$ GPa. Of course, in making such estimates, no account is taken of any effect of the size of the region of stress concentration, so that there is no consideration of the nucleation and growth of kink bands, but the similarity of these two numbers nevertheless suggests that the true strength may be of this order.

For the grade B material, the corresponding estimates lead to values of about 2.7 GPa for $d = 1.7$ mm and 2.1 GPa for $d = 1.2$ mm. In this case, however, it is known that the microstructure of the region effectively being tested (ie the periphery of the specimen) was different for the two geometries. For the larger specimen diameter, the periphery was effectively pore-free, leading to a strength close to that of the grade A material. When the pore-free region had been removed, however, the strength being measured would be more representative of the bulk of the material, which was quite porous, and it can be seen that this is appreciably lower.

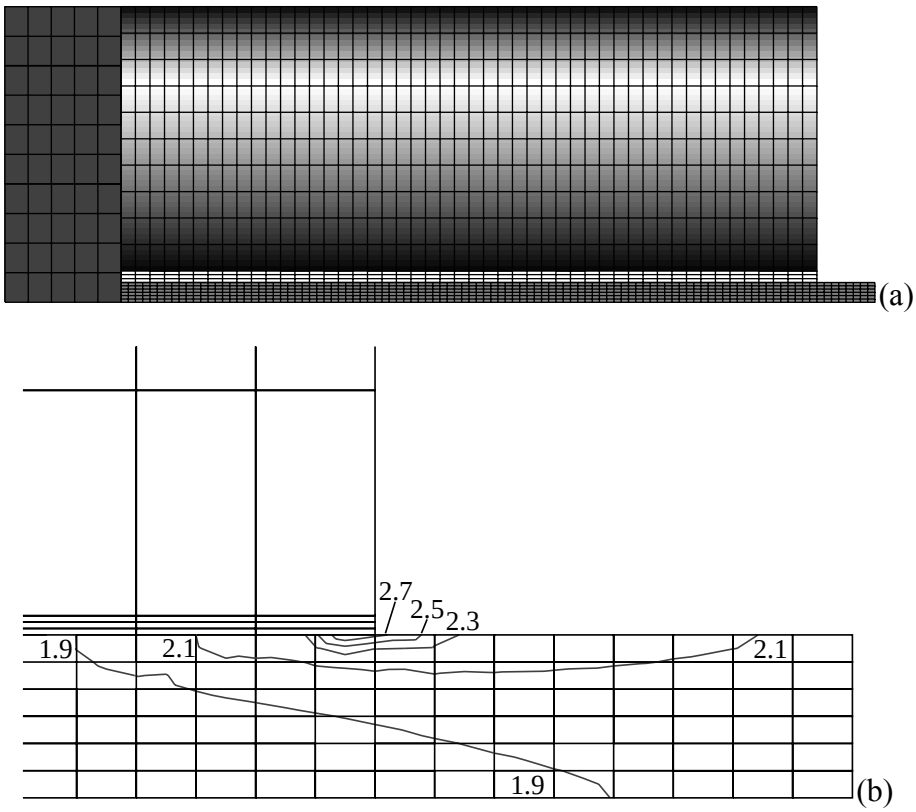

Figure 6 (a) FEM mesh for study of the influence of test geometry on the stress distribution, showing the specimen (bottom), adhesive layer and steel cylinder, with the hardened steel plate on the left, and (b) expanded view of the region where the specimen enters the cylinder, showing contours of axial stress within the specimen, for a remote applied stress of 2 GPa.

4.2 Stress Concentrating Effect of Pores

In order to study the expected effect of the pores in material of this type, FEM meshes incorporating voids were generated within a material modeled as an anisotropic continuum.

These voids were elliptical in shape, with the long axis aligned parallel to the loading direction. The effects of hole aspect ratio were studied. Fig.8 shows how the stress concentration factor for the peak normal stress along the loading axis, and the peak shear stress on planes parallel to the loading axis, are predicted to vary with pore aspect ratio. The peak in shear stress occurs immediately adjacent to the hole and decays rapidly with distance away from it.

These results confirm that pores of the type present in the grade B material would indeed be expected to have a significant effect in reducing the compressive strength. This could be deduced either from the concentration of axial stress adjacent to the holes (a stress concentration factor of about 1.3 being predicted) or from the fact that significant shear stresses parallel to the fibre axis (~10% of the applied stress, ie ~200 MPa) arise near the ends of the pores. It is not really possible to quantify the expected effects of these stresses on the strength without considering the mechanisms of failure in more detail, particularly since they occur in very small volumes of material, but it seems clear that these predicted changes in stress state due to the presence of the pores would be expected to effect a significant reduction in measured strength.

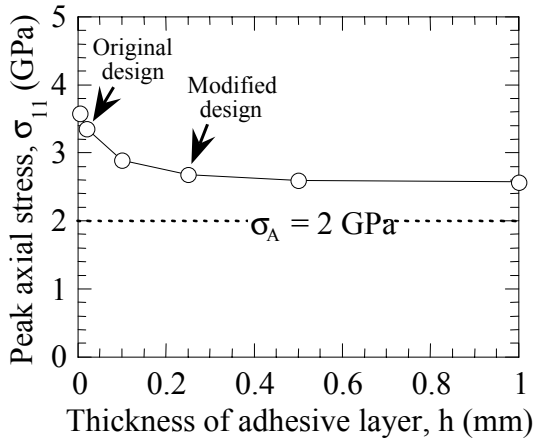

Figure 7 Predicted dependence of the peak axial stress within the specimen, for the system shown in Fig.6, on the thickness of the layer of adhesive between the specimen and the steel cylinder.

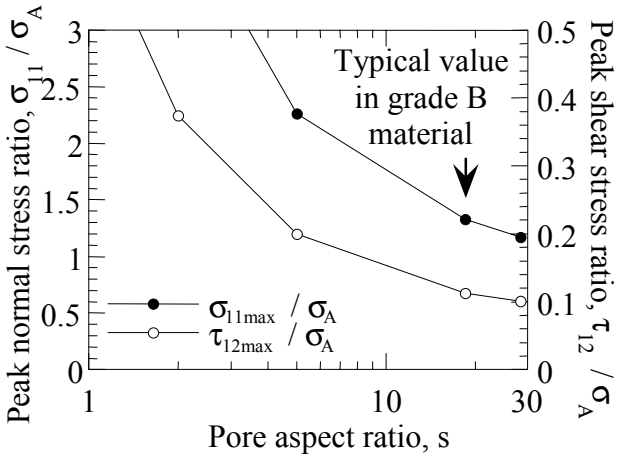

Figure 8 Predicted dependence of the stress concentration factors for peak axial and shear stresses within the composite, in the vicinity of a pore, on the pore aspect ratio.

5. CONCLUSIONS

The following conclusions may be drawn from this work.

(a) Work has been carried out on two grades of pultruded composite rod. These both exhibited good fibre alignment, but grade B contained elongated pores in the central region whereas grade A was effectively pore-free.

(b) Fibre alignment was characterized via measurements of fibre aspect ratios in polished sections inclined to the alignment axis and by using a a recently-developed image analysis technique. Both methods confirmed that the two grades exhibited excellent alignment, with virtually no fibres misaligned by more than about 1˚. Data from the image analysis method indicated that the alignment was slightly better in grade A than in grade B.

(c) Compressive strength measurements were made (i) on as-received rods (1.7 mm diameter), with a thin (40 μm) adhesive layer and (ii) on rods reduced in diameter to 1.2 mm, with a thick (300 μm) adhesive layer. A pronounced tendency was noted for failure to occur where the specimen entered the grips, particularly with the larger diameter specimens. The

failure mechanism was via kink band formation in all cases. There were indications that the kink bands nucleated preferentially at the free surface of the specimen.

(d) FEM modeling indicated significant stress concentrations in the region where the specimen entered the grips. This was more pronounced with the thinner adhesive layer. From stress concentration factors for the two geometries, the true compressive strength was estimated for each grade of material. For the larger diameter specimens of grade B material, the outer, pore-free region was effectively being tested, rather than the porous interior.

(e) Deduced true compressive strengths were about 2.7-2.8 GPa for the pore-free (grade A) material and 2.1 GPa for the porous (grade B core) material. This difference may be partly a consequence of the slightly inferior fibre alignment in the grade B material. However, it seems likely that there is also a substantial reduction in strength resulting from the presence of the pores. FEM modeling of an anisotropic continuum containing elongated voids showed that the stress state changes predicted to occur as a consequence of the presence of the pores would be likely to have a significant effect in promoting compressive failure.

ACKNOWLEDGEMENTS

This work was carried out as part of a studentship supported by the EPSRC, within a programme involving Hexcel Composites, British Aerospace, DERA and Neptco. The authors are grateful for useful discussions with P.M.McClellan and S.O'Meara, of Neptco, with Dr.J.Ball, of British Aerospace, and with Prof.N.A.Fleck and Dr.M.P.F.Sutcliffe, of Cambridge University.

REFERENCES

1. B. Budiansky and N. A. Fleck, *Compressive Failure of Fibre Composites*, J. Mech. Phys. Sol., **41** (1993), pp. 183-211.

2. A. S. Argon, *Fracture of Composites*, Vol. 1, Academic Press, New York, (1972).

3. B. W. Rosen, *Strength of Uniaxial Fibrous Composites*, in *Mechanics of Composite Materials*, F. W. Wendt, H. Liebowitz and N. Perrone (Eds.), Pergamon Press, Oxford, (1970), pp. 621-651.

4. M. R. Piggott and P. Wilde, *Compressive Strength of Aligned Steel Reinforced Epoxy Resin*, J. Mat. Sci., **15** (1980), pp. 2811-2815

5. M. R. Piggott and B. Harris, *Compression Strength of Carbon, Glass and Kevlar 49 Fibre Reinforced Polyester Resins*, J. Mat. Sci., **15** (1980), pp. 2523-2538.

6. M. R. Wisnom, *The Effect of Fibre Misalignment on the Compressive Strength of Unidirectional Carbon Fibre / Epoxy*, Composites, **21** (1990), pp. 403-407.

7. A. L. Highsmith, J. J. Davis and K. L. E. Helms, *The Influence of Fiber Waviness on the Compressive Behavior of Unidirectional Continuous Fiber Composites*, in *Composite Materials, Testing and Design, ASTM STP 1120*, G. C. Grimes (Ed.), Vol. 1120, ASTM, Philadelphia, (1992), pp. 20-36.

8. P. M. Jelf and N. A. Fleck, *Compression Failure Mechanisms in Unidirectional Composites*, J. Comp. Mats., **26** (1992), pp. 2706-2726.

9. J. G. Häberle and F. L. Matthews, *An Improved Technique for Compresion Testing of Fibre-Reinforced Plastics; Development and Results*, Composites, **25** (1994), pp. 358-371.

10. M. R. Piggott, *The Effect of Fibre Waviness on the Mechanical Properties of Unidirectional Fibre Composites - A Review*, Comp. Sci. Tech, **53** (1995), pp. 201-205.

11. M. P. F. Sutcliffe and N. A. Fleck, *Effect of Geometry on Compressive Failure of Notched Composites*, Int. J. Fracture, **59** (1993), pp. 115-132.

12. W. S. Slaughter and N. A. Fleck, *Microbuckling of Fiber Composites with Random Initial Fiber Waviness*, J. Mech. Phys. Solids., **42** (1994), pp. 1743-1766.

13. N. A. Fleck and J. Y. Shu, *Microbuckle Initiation in Fibre Composites: a Finite Element Study.*, J. Mech. Phys. Solids, **43** (1995), pp. 1887-1918.

14. V. V. Kozey, *Fibre Strength-Dominated Failure Mode In Unidirectional Composites Under Compression*, J. Mat. Sci. Lets, **12** (1993), pp. 48-52.

15. R. R. Effendi, J.-J. Barrau and D. Guedra-Degeorges, *Failure Mechanism Analysis Under Compression Loading of Unidirectional Carbon/Epoxy Composites using Micromechanical Modelling*, Composite Structures, **31** (1995), pp. 87-98.

16. J. E. Spowart and T. W. Clyne, *The Failure Mechanism in Monofilament-Reinforced Titanium under Axial Compression*, in ICCM-11 (1997), Gold Coast, M. L. Scott (Ed.) Vol. 3, pp. 467-478.

17. J. E. Spowart and T. W. Clyne, *Deformation and Failure of Monofilament–Reinforced Titanium under Axial Compressive Loading*, Key Eng. Mats., **127-131** (1997), pp. 833-842.

18. J. E. Spowart and T. W. Clyne, *The Axial Compressive Failure of Titanium Reinforced with Silicon Carbide Monofilaments*, Acta Mater., **47** (1998), pp. 671-687.

19. M. Vincent and J. F. Agassant, *Experimental Study and Calculations of Short Glass Fiber Orientation in a Center Gated Molded Disk*, Polymer Composites, **7** (1986), pp. 76-83.

20. S. W. Yurgartis, *Measurement of Small Angle Fiber Misalignments in Continuous Fiber Composites.*, Comp. Sci. and Tech., **30** (1987), pp. 279-293.

21. C. J. Creighton, M. P. F. Sutcliffe and T. W. Clyne, *A Multiple Field Image Analysis Procedure for Characterisation of Fibre Alignment in Composites*, Comp. Sci. & Techn., submitted (1999).

22. F. R. Shanley, *Inelastic Column Theory*, J. Aeronautical Sciences, **14** (1947), pp. 261-268.

23. F. R. Shanley, *Strength of Materials*, McGraw-Hill, New York, NY USA, (1957).

24. S. P. Timoshenko and J. M. Gere, *Theory of Elastic Stability*, 2 edn., McGraw-Hill Book Co., New York, NY USA, (1961).

25. J. D. Eshelby, *The Determination of the Elastic Field of an Ellipsoidal Inclusion and Related Problems*, Proc. Roy. Soc. London, Ser. A, **241** (1957), pp. 376-396.

26. T. W. Clyne and P. J. Withers, *An Introduction to Metal Matrix Composites*, Cambridge University Press, Cambridge, (1993).

27. J. E. Spowart, *The Compressive Failure of SiC Monofilament Reinforced Titanium*, PhD thesis, Univ. of Cambridge (1998).